

CONSTRAINED RUNS ALGORITHM AS A LIFTING OPERATOR FOR THE BOLTZMANN EQUATION

YNTE VANDERHOYDONC* AND WIM VANROOSE†

Abstract. Lifting operators play an important role in starting a kinetic Boltzmann model from given macroscopic information. The macroscopic variables need to be mapped to the distribution functions, mesoscopic variables of the Boltzmann model. A well-known numerical method for the initialization of Boltzmann models is the Constrained Runs algorithm. This algorithm is used in literature for the initialization of lattice Boltzmann models, special discretizations of the Boltzmann equation. It is based on the attraction of the dynamics toward the slow manifold and uses lattice Boltzmann steps to converge to the desired dynamics on the slow manifold. We focus on applying the Constrained Runs algorithm to map density, average flow velocity, and temperature, the macroscopic variables, to distribution functions. Furthermore, we do not consider only lattice Boltzmann models. We want to perform the algorithm for different discretizations of the Boltzmann equation and consider a standard finite volume discretization.

Key words. Lifting operator, initialization, missing data, kinetic Boltzmann models, macroscopic partial differential equations, finite volume discretization, Constrained Runs

AMS subject classifications. 76P05, 82C40, 35K45, 35K57

1. Introduction. Fluid dynamics can typically be described by different levels of accuracy. One distinguishes between micro-, meso-, and macroscopic scales. Macroscopic partial differential equations (PDEs) model only a few low order velocity moments and are therefore not that accurate to describe interactions between particles. Well-known macroscopic equations for the modeling of fluid dynamics are the Euler and Navier–Stokes equations. However, when a detailed description is necessary, a microscopic model is used. These individual-based models take the particle collision physics into account. The Boltzmann equation can be used to describe kinetic models, that are ubiquitous to model at this scale, by modeling distribution functions in phase space.

We focus on space, time, and velocity discretizations of the Boltzmann equation. The initialization of such a discretized Boltzmann equation requires a lifting operator when only macroscopic information is available. This operator defines a mapping between macroscopic and microscopic/mesoscopic variables such that the distribution functions of the discretized Boltzmann equation can be built from the given macroscopic information. The concept of a lifting operator in a multiscale context was introduced by Kevrekidis et al. in the equation-free framework to couple different scales in a dynamical system [15]. Similar ideas were introduced in the heterogeneous multiscale methods framework that starts from a predetermined incomplete form for the macroscopic model and estimates the needed data for the incomplete macroscopic model from the microscopic model [6].

Lots of previous work in the literature is based on the initialization of lattice Boltzmann models (LBMs), special discretizations of the Boltzmann equation [19, 31]. Lifting operators for LBMs are considered in [22, 23, 24, 26, 27, 28, 30] where a given initial density is mapped to distribution functions. The Chapman–Enskog expansion is built for such model problems in [22]. This analytical expansion is first introduced

*Dept. Mathematics and Computer Science, Universiteit Antwerpen, Middelheimlaan 1, 2020 Antwerpen, Belgium (ynite.vanderhoydonc@uantwerp.be).

†Dept. Mathematics and Computer Science, Universiteit Antwerpen, Middelheimlaan 1, 2020 Antwerpen, Belgium (wim.vanroose@uantwerp.be).

in [4] to solve the Boltzmann equation. Furthermore, [22], [23], [24], and [26] apply the Constrained Runs (CR) algorithm to LBMs. Originally, the CR algorithm is introduced by Gear et al. [7] to map macroscopic initial variables to missing microscopic variables for stiff singularly perturbed ordinary differential equations (ODEs). This algorithm is based on the attraction of the dynamics toward the slow manifold. The dynamics on this slow manifold can be parameterized by only macroscopic variables such as the density. The higher order velocity moments become slaved functionals of the density in the LBM context. [27] compares the Chapman–Enskog expansion with the CR algorithm for hybrid model problems with given initial density. [28] constructs the numerical Chapman–Enskog expansion as a lifting operator for these model problems. This numerical Chapman–Enskog expansion is based on a combination of the Chapman–Enskog expansion and the CR algorithm. It finds the coefficients of the Chapman–Enskog expansion numerically based on the CR algorithm. This reduces the number of unknowns in the lifting since it only finds the coefficients of the expansion rather than the full state of distribution functions. A review of these lifting operators for LBMs with an initial density as macroscopic variable is given in [30]. A generalization of the numerical Chapman–Enskog expansion is made in [29] where both density and momentum are considered to be given at initialization.

In this paper, we apply the Constrained Runs algorithm on a finite volume discretization of the one-dimensional Boltzmann equation which maps macroscopic information, namely density, average flow velocity, and temperature, to distribution functions of the discretized Boltzmann equation. The intention of this generalization is to deal with multiple given macroscopic variables. We do not conserve only the density but also average flow velocity and temperature to work towards more realistic physical systems. This lifting operator is constructed to deal, for example, with missing data in a hybrid kinetic and macroscopic PDE model for laser ablation. In laser ablation, a complex interplay between various processes determines the outcome of a laser beam hitting on a solid target [3]. First, the target is heated by the laser and the heat is transported over the material. The material then starts to melt. Above the surface of the melted material there is evaporation and the particles escape according to a certain velocity distribution. Due to the strong evaporation, the particles right above the melt/gas interface are not in an equilibrium state. This thin layer above the surface is known as the Knudsen layer which cannot be described by a macroscopic PDE. It requires a detailed kinetic model such as the Boltzmann equation. Once away from the surface the plume expansion can be described by a macroscopic PDE model. The challenge is to couple the models describing the different physical processes in a mathematical correct way.

We first applied the generalization of the CR algorithm in [29] for a small number of velocities to deal with the conservation of density and momentum in lattice Boltzmann problems.

The outline of this paper is as follows. Section 2 contains the different levels of description that will be used throughout the paper. The mesoscopic level uses the discretized version of the Boltzmann equation while the macroscopic equivalent PDEs are the Euler and Navier–Stokes equations. Section 3 describes the Constrained Runs algorithm. The origin of the Constrained Runs algorithm is included in section 3.1. Section 3.2 contains the application of Constrained Runs to lattice Boltzmann models. The generalization to different discretizations of the Boltzmann equation and multiple conserved moments is outlined in section 3.3. Numerical results can be found in section 4 where the lifting operator is tested in a setting of restriction and lifting.

A conclusion and outlook are included in section 5.

2. Different levels of description. This section introduces models with different levels of description that will be used throughout this paper. The mesoscopic scale is described by a finite volume discretization of the Boltzmann equation and will be discussed in section 2.1. The macroscopic scale uses discretized partial differential equations (PDEs) to describe the evolution of a few low order velocity moments in section 2.2.

2.1. Mesoscopic description. Kinetic models make use of the Boltzmann equation [19] that describes the evolution of a distribution function $f(\mathbf{x}, \mathbf{v}, t)$ (function space $C_{\mathbb{R}}^2(D)$) that counts the number of particles or individuals in point $\mathbf{x} \in D_{\mathbf{x}} \subset \mathbb{R}^n$, $n \in \mathbb{N}_0$, with a velocity $\mathbf{v} \in D_{\mathbf{v}} \subset \mathbb{R}^n$, at time $t \geq 0$. The equation is given by (without external forces, with Bhatnagar–Gross–Krook (BGK) collision term [14])

$$\frac{\partial}{\partial t} f(\mathbf{x}, \mathbf{v}, t) + \mathbf{v} \cdot \frac{\partial}{\partial \mathbf{x}} f(\mathbf{x}, \mathbf{v}, t) = \omega(f^{eq}(\mathbf{x}, \mathbf{v}, t) - f(\mathbf{x}, \mathbf{v}, t)). \quad (2.1)$$

The Maxwell–Boltzmann equilibrium distribution is

$$f^{eq}(\mathbf{x}, \mathbf{v}, t) = n \left(\frac{m}{2\pi k_B T} \right)^{d/2} e^{-\frac{m(\mathbf{v} - \mathbf{u})^2}{2k_B T}},$$

where k_B is the Boltzmann constant, d the number of spatial dimensions, m the molecular mass, n the number density, T the temperature, and \mathbf{u} the average flow velocity. The macroscopic variables are defined by [18]

$$\begin{aligned} n(\mathbf{x}, t) &= \int f(\mathbf{x}, \mathbf{v}, t) d\mathbf{v}, \\ \rho(\mathbf{x}, t) &= \int m f(\mathbf{x}, \mathbf{v}, t) d\mathbf{v}, \\ \rho(\mathbf{x}, t) \mathbf{u}(\mathbf{x}, t) &= \int m \mathbf{v} f(\mathbf{x}, \mathbf{v}, t) d\mathbf{v}, \\ T(\mathbf{x}, t) &= \frac{1}{d\rho R} \int m \|\mathbf{v} - \mathbf{u}\|^2 f(\mathbf{x}, \mathbf{v}, t) d\mathbf{v}, \end{aligned} \quad (2.2)$$

with $\|\cdot\|$ the two-norm and $R = k_B/m$ the specific gas constant.

The BGK collision term approximation represents a relaxation towards equilibrium with a relaxation parameter ω and an associated time scale $\tau = 1/\omega$. Atomic collisions are taken into account by the relaxation frequency ω [1] given by

$$\omega = \rho \frac{k_B}{m} \frac{T}{\mu}, \quad (2.3)$$

with μ the viscosity of the gas which is determined by

$$\mu = \mu_{\text{ref}} \left(\frac{T}{T_{\text{ref}}} \right)^{\omega_{\mu}}.$$

ω_{μ} represents the viscosity index of the considered gas [2], and μ_{ref} and T_{ref} are the reference viscosity and temperature determined experimentally.

Consider the one-dimensional Boltzmann equation in space

$$\frac{\partial f}{\partial t} + v \frac{\partial f}{\partial x} = \omega(f^{eq} - f).$$

The velocity discretization of the Boltzmann equation results into a set of N_v linear advection equations, with N_v the number of velocity directions and $v_i = v_0 + i\Delta v$, $i \in \{0, \dots, N_v - 1\}$ and $\Delta v = (v_{\max} - v_{\min})/N_v$.

$$\frac{\partial f_i}{\partial t} + v_i \frac{\partial f_i}{\partial x} = \omega(f_i^{eq} - f_i). \quad (2.4)$$

The discretization of the equilibrium distribution function is outlined below and is based on the algorithm described in [9]. We look for the equilibrium distribution function f_i^{eq} in the general form

$$f_i^{eq} = A \exp(-B^2(v_i - D)^2), \quad (2.5)$$

which has to approach the Maxwell-Boltzmann distribution as the increment Δv tends to zero. A , B , and D are derived from the conservation equations of mass, momentum, and energy, which are defined by

$$\begin{aligned} \Delta v \sum_{i=0}^{N_v-1} f_i &= n = \Delta v \sum_{i=0}^{N_v-1} f_i^{eq}(A, B, D), \\ \Delta v \sum_{i=0}^{N_v-1} v_i f_i &= nu = \Delta v \sum_{i=0}^{N_v-1} v_i f_i^{eq}(A, B, D), \\ \Delta v \sum_{i=0}^{N_v-1} (v_i - u)^2 f_i &= \frac{nk_B T}{m} = \Delta v \sum_{i=0}^{N_v-1} (v_i - u)^2 f_i^{eq}(A, B, D). \end{aligned}$$

From this follows

$$A = \frac{n}{R_0}, \quad R_1 = 0, \quad R_2 - \frac{R_0 k_B T}{m} = 0,$$

where

$$R_j = \Delta v \sum_{i=0}^{N_v-1} (v_i - u)^j \exp(-B^2(v_i - D)^2),$$

from which A , B , and D are obtained through a Newton algorithm on this set of equations with the initial approximation of $B = \sqrt{m/(2k_B T)}$ and $D = u$.

For the space and time discretization, we consider the one discussed in [16] by Lafitte and Samaey. It represents a finite volume discretization of the Boltzmann equation. Consider a grid which is uniform in time with time step Δt and a spatial grid with space step Δx :

$$C_j = [x_{j-\frac{1}{2}}, x_{j+\frac{1}{2}}), \quad 1 \leq j \leq N,$$

centered in x_j with $x_j = j\Delta x$,

$$T_k = [t^k, t^{k+1}), \quad k \geq 0, \quad t^k = k\Delta t.$$

By integrating (2.4) on a cell $M_{j,k} = C_j \times T_k$, this results in

$$\begin{aligned} f_i(x_j, t^{k+1}) = & f_i(x_j, t^k) - \frac{\Delta t}{\Delta x} \left(\phi(f)_{i,j+1/2}^k - \phi(f)_{i,j-1/2}^k \right) \\ & + \Delta t \omega \left(f_i^{eq}(x_j, t^k) - f_i(x_j, t^k) \right), \end{aligned}$$

with upwind fluxes

$$\phi_u(f)_{i,j+1/2}^k = \begin{cases} v_i f_i(x_j, t^k), & v_i \geq 0, \\ v_i f_i(x_{j+1}, t^k), & v_i < 0, \end{cases}$$

or centered fluxes

$$\phi_c(f)_{i,j+1/2}^k = v_i \frac{f_i(x_{j+1}, t^k) + f_i(x_j, t^k)}{2}.$$

Different discretizations of the Boltzmann equation are given in [17]. It represents a similar explicit finite volume scheme and a linearized implicit scheme to compute steady states. It focuses on the positivity of solutions, the conservation of moments, and the dissipation of entropy.

2.2. Macroscopic description. When the phenomena of fluid dynamics that one wants to describe are macroscopic, the fluid is regarded as a continuous medium. The fundamental equations to describe the motion of the fluid are the Euler and Navier–Stokes equations [5]. It can be shown that these are macroscopic equivalents of the Boltzmann equation. For this, the Chapman–Enskog expansion can be used [4, 31].

The Euler equations represent conservation of mass, momentum, and energy while the Navier–Stokes equations extends these equations to include the viscosity of the fluid.

2.3. Initialization. Suppose there is some initial data based on macroscopic variables, like density, average flow velocity, and temperature. An important question is how to start simulating a Boltzmann model, which is based on distribution functions, given initial macroscopic information. Starting the Boltzmann scheme includes some arbitrariness since there are many possible distribution functions which have the same velocity moments. We need to create a mapping from the macroscopic velocity moments to distribution functions. For this a lifting operator is necessary. Section 3 describes the Constrained Runs algorithm that is used in this paper as a lifting operator for the initialization of Boltzmann models. It is a known algorithm for the initialization of lattice Boltzmann models. This paper generalizes it to apply it for different discretizations of the Boltzmann equation and multiple conserved velocity moments.

3. Constrained Runs algorithm. The Constrained Runs (CR) algorithm is a numerical method based on the attraction of the dynamics toward the slow manifold. The origin of the CR algorithm in systems of ODEs is described in section 3.1. The application to LBMs with given initial density is included in section 3.2. Here, we immediately present the generalized CR algorithm for LBM problems. The generalization to different discretizations of the Boltzmann equation and multiple conserved moments (density, average flow velocity, and temperature) is discussed in section 3.3.

3.1. Origin of Constrained Runs algorithm. The CR algorithm finds its origin in systems of ODEs [7]. A review of this work is given in [30] and summarized below. Given system

$$\begin{aligned}\frac{d\mathbf{r}(t)}{dt} &= p(\mathbf{r}(t), \mathbf{s}(t)), \\ \frac{d\mathbf{s}(t)}{dt} &= q(\mathbf{r}(t), \mathbf{s}(t)),\end{aligned}\tag{3.1}$$

where only the initial condition for \mathbf{r} , namely $\mathbf{r}(0) = \mathbf{r}_0$, is given. The aim is to find $\mathbf{s}(0) = \mathbf{s}_0$ such that the initial condition $(\mathbf{r}_0, \mathbf{s}_0)$ lies on (or close to) the slow manifold. The latter can be formulated by the function $\mathbf{s}_0 = \mathbf{s}(\mathbf{r}_0)$.

Gear et al. [7] proposed to obtain the \mathbf{s} -value from equation

$$\frac{d^{m+1}\mathbf{s}(t=0)}{dt^{m+1}} = 0,\tag{3.2}$$

the smoothness condition, with $m = 0, 1, \dots$ that can be approximated by a forward difference

$$\Delta^{m+1}\mathbf{s}(t) \approx \Delta t^{m+1} \frac{d^{m+1}\mathbf{s}(t)}{dt^{m+1}}.\tag{3.3}$$

It can be shown that this difference approximation used in the CR algorithm can be interpreted as a backward extrapolation [25]. It corresponds with a backward extrapolation in time based on a polynomial of degree m that passes through the values \mathbf{s}_k with $k = 1, \dots, m+1$ while the known variable \mathbf{r} is reset to its original initial value \mathbf{r}_0 . The used coefficients of the forward finite difference formulas at time t are listed in Table 3.1 for different degrees of m .

m	$t + \Delta t$	$t + 2\Delta t$	$t + 3\Delta t$	$t + 4\Delta t$
0	1	0	0	0
1	2	-1	0	0
2	3	-3	1	0
3	4	-6	4	-1

TABLE 3.1

Coefficients of the forward finite difference formulas at time t for different degrees of m in (3.3).

For example, for $m = 1$, this formula corresponds to $\Delta t^2 \frac{d^2\mathbf{s}(t)}{dt^2} \approx \mathbf{s}(t) - 2\mathbf{s}(t + \Delta t) + \mathbf{s}(t + 2\Delta t)$. Using (3.2), this leads to $\mathbf{s}(t) = 2\mathbf{s}(t + \Delta t) - \mathbf{s}(t + 2\Delta t)$ from which the coefficients can be obtained.

The general CR algorithm for a constant extrapolation, $m = 0$, is given in Algorithm 1.

Similar algorithms can be constructed for higher degrees of m by advancing the model during more time steps and using (3.2) for different values of m .

3.2. Constrained Runs algorithm applied to lattice Boltzmann models.

The CR scheme [7] is a fixed point iteration scheme that computes the full state of a microscopic time simulator on (or close to) the slow manifold corresponding to the given macroscopic variables.

Consider an LBM problem in a D1Q3 setting (one spatial dimension, three velocity directions $v_i = c_i\Delta x/\Delta t$, $c_i = i$, $i \in \{-1, 0, 1\}$). The lattice Boltzmann equation (LBE) is

$$f_i(x + c_i\Delta x, t + \Delta t) = (1 - \omega)f_i(x, t) + \omega f_i^{eq}(x, t).$$

Algorithm 1 Constrained Runs for a constant extrapolation in time in the system of ODEs (3.1)

Require: Initial condition $\mathbf{r}(0) = \mathbf{r}_0$

Choose \mathbf{s}_0 , norm $\|\cdot\|$ and a tolerance θ

repeat

Advance the model with one time step Δt :

\mathbf{r}_1 and \mathbf{s}_1 at time $t = \Delta t$

Difference approximation $\Delta \mathbf{s}_0 = \mathbf{s}_1 - \mathbf{s}_0$

$\mathbf{s}_0 \leftarrow \mathbf{s}_0 + \Delta \mathbf{s}_0$

Reset \mathbf{r} to \mathbf{r}_0 , the given initial condition

until $\|\Delta \mathbf{s}_0\| < \theta$

This is a special discretization of the Boltzmann equation (2.1) [19, 31]. The equilibrium distributions are given by $f_i^{eq}(x, t) = \frac{1}{3}\rho(x, t)$, $i \in \{-1, 0, 1\}$ [21] in which the particle density $\rho(x, t)$ is defined as the zeroth order moment of the distribution functions $\rho(x, t) = \sum_{i \in \{-1, 0, 1\}} f_i(x, t)$. These equilibrium distributions correspond to a local diffusive equilibrium.

We now describe the application of Constrained Runs to LBMs [22, 24] when we assume that a slow manifold exists in this context.

The CR algorithm sets a few LBM steps after which the density is reset. The number of LBM steps is related to the order m and determines the accuracy of the resulting lifted distribution function. Doing only one LBM step corresponds to a constant extrapolation in time.

The CR procedure for LBMs iterates upon the higher order moments ϕ and ξ , momentum and energy, given a density $\rho_0 = \rho(\mathbf{x}, 0)$. It is equivalent to determine $\mathbf{f} := \{\mathbf{f}_1; \mathbf{f}_0; \mathbf{f}_{-1}\}$ or $\mathcal{M} := \{\rho; \phi; \xi\}$ since the velocity moments are related via moment matrix $M \in \mathbb{R}^{3 \times 3}$:

$$\begin{pmatrix} \rho \\ \phi \\ \xi \end{pmatrix} = \begin{pmatrix} 1 & 1 & 1 \\ 1 & 0 & -1 \\ \frac{1}{2} & 0 & \frac{1}{2} \end{pmatrix} \begin{pmatrix} f_1 \\ f_0 \\ f_{-1} \end{pmatrix} = M \begin{pmatrix} f_1 \\ f_0 \\ f_{-1} \end{pmatrix}, \quad (3.4)$$

or, in shorthand, $\mathcal{M} = M\mathbf{f}$. Denote M^0 as

$$M^0 = \begin{pmatrix} 1 & 1 & 1 \\ 0 & 0 & 0 \\ 0 & 0 & 0 \end{pmatrix} = \text{diag}(1, 0, 0)M.$$

M^0 represents the part of matrix M that produces the density which should be conserved in the CR algorithm.

To apply CR, the missing moments are written as

$$\mathbf{s} = \begin{pmatrix} \phi \\ \xi \end{pmatrix},$$

a long vector $\mathbf{s} \in \mathbb{R}^{2N}$, the variable $\mathbf{r}_0 = \boldsymbol{\rho}_0 \in \mathbb{R}^N$ denotes the known initial condition, with N the number of spatial grid points.

The vector $\mathbf{s}^{(k)}$ denotes the k -th iterate of the CR algorithm and the iterations are related by

$$\mathbf{s}^{(k+1)} = \mathcal{C}_m \left(\mathbf{r}_0, \mathbf{s}^{(k)} \right), \quad (3.5)$$

where \mathcal{C}_m denotes one step of the CR algorithm and m is related to the order of the time derivative that is set to zero in equation (3.2).

Below, this paper presents the CR algorithm in a general setting. We write the CR iteration in terms of the distribution functions \mathbf{f} rather than missing moments ϕ and ρ . The algorithm generates a sequence of moments $\mathcal{M}^{(k)}$ with $k = 0, 1, 2, \dots$ and $\mathcal{M}^{(0)} = \{\rho_0; (\frac{1}{3} - \frac{1}{3})\rho_0; \frac{1}{2}(\frac{1}{3} + \frac{1}{3})\rho_0\}$ the initial guess corresponding to the equilibrium distribution function. In this sequence, the zeroth moment $\mathcal{M}_0^{(k)}$ is always the initial density ρ_0 and $\mathcal{M}_1^{(k)} = \phi^{(k)}$ and $\mathcal{M}_2^{(k)} = \xi^{(k)}$ converge to the slaved state. The iteration consists of two steps. First, $\mathcal{M}^{(k)}$ is transformed to $\mathbf{f}^{(k)}$ using (3.4) and this is used as an initial state of an LBM that is evolved over $m + 1$ time steps. This gives states $\mathbf{f}^{(k)}(\Delta t), \mathbf{f}^{(k)}(2\Delta t), \dots, \mathbf{f}^{(k)}((m + 1)\Delta t)$ that can be converted to $\mathcal{M}^{(k)}(\Delta t), \mathcal{M}^{(k)}(2\Delta t), \dots, \mathcal{M}^{(k)}((m + 1)\Delta t)$. With these states we can generate

$$\mathcal{M}_i^{(k)\text{pre}} = \sum_{j=1}^{m+1} w_j \mathcal{M}_i^{(k)}(j\Delta t) \quad \text{for } i = 1, 2, \quad (3.6)$$

the improved higher order moments where we add a superscript “pre” to denote that this is the value before resetting the density. The underlying idea is that $\mathcal{M}^{(k)\text{pre}}$ is chosen such that combined with $\mathcal{M}^{(k)}(j\Delta t)$ it satisfies the smoothness condition (3.2) by letting the weights w_j correspond to the coefficients of the forward finite difference formula in (3.3) given in Table 3.1.

For the ease of analysis, we also apply the backward interpolation formula to the zeroth moment. Now, we can write for all moments that

$$\mathcal{M}^{(k)\text{pre}} = \sum_{j=1}^{m+1} w_j \mathcal{M}^{(k)}(j\Delta t). \quad (3.7)$$

To get the next iterate we introduce a reset step that sets the zeroth moment to ρ_0 such that the density is conserved.

$$\mathcal{M}^{(k+1)} = \begin{pmatrix} \rho_0 \\ \mathcal{M}_1^{(k)\text{pre}} \\ \mathcal{M}_2^{(k)\text{pre}} \end{pmatrix}.$$

This reset is the second step in the iteration. The two steps can be written as

$$\begin{aligned} \mathcal{M}^{(k+1)} &= \begin{pmatrix} 0 & 0 & 0 \\ 0 & 1 & 0 \\ 0 & 0 & 1 \end{pmatrix} \mathcal{M}^{(k)\text{pre}} + \begin{pmatrix} 1 & 0 & 0 \\ 0 & 0 & 0 \\ 0 & 0 & 0 \end{pmatrix} \begin{pmatrix} \rho_0 \\ 0 \\ 0 \end{pmatrix}, \\ &= (M - M^0) \mathbf{f}^{(k)\text{pre}} + M^0 \mathbf{f}^0, \end{aligned}$$

where \mathbf{f}^0 is an initial distribution function that has ρ_0 as density. Reordering leads to

$$\begin{aligned} M \mathbf{f}^{(k+1)} &= (M - M^0) \mathbf{f}^{(k)\text{pre}} + M^0 \mathbf{f}^0, \\ \mathbf{f}^{(k+1)} &= M^{-1} \left[(M - M^0) \mathbf{f}^{(k)\text{pre}} + M^0 \mathbf{f}^0 \right], \\ \mathbf{f}^{(k+1)} &= (I - M^{-1} M^0) \mathbf{f}^{(k)\text{pre}} + M^{-1} M^0 \mathbf{f}^0. \end{aligned}$$

In conclusion we can write

$$\mathbf{f}^{(k+1)} = (I - M^{-1}M^0) \left(\sum_{j=1}^{m+1} w_j \mathbf{f}^{(k)}(j\Delta t) \right) + M^{-1}M^0 \mathbf{f}^0. \quad (3.8)$$

The convergence rate and stability of this iteration depend on the order m and the coefficients w_j from Table 3.1.

Note that the operator $P := I - M^{-1}M^0$ that appears in the first term of (3.8) is a projection operator. Indeed, we can write $M^{-1}M^0 = M^{-1}\text{diag}(1, 0, 0)M$ and it is now easy to see that $(M^{-1}M^0)^2 = M^{-1}\text{diag}(1, 0, 0)MM^{-1}\text{diag}(1, 0, 0)M = M^{-1}M^0$. As a result $P^2 = P$.

The interpretation of (3.8) is that the first term projects the state on the space orthogonal to the space spanned by the lowest order moments. The second term adds the original components in the space of the low order moments, here the density.

In general, equation (3.5) is nonlinear and the fixed point can be found by a Newton iteration [26]. This means solving

$$g_m(\mathbf{r}_0, \mathbf{s}) := \mathbf{s} - \mathcal{C}_m(\mathbf{r}_0, \mathbf{s}) = 0, \quad (3.9)$$

for a given macroscopic value \mathbf{r}_0 . Newton's method gives an update to the guesses as follows

$$\mathbf{s}^{(k+1)} = \mathbf{s}^{(k)} + \delta \mathbf{s}^{(k)},$$

where the corrections $\delta \mathbf{s}^{(k)}$ are found by solving the linear system

$$\begin{aligned} A(\mathbf{r}_0, \mathbf{s}^{(k)}) \delta \mathbf{s}^{(k)} &= \frac{\partial g_m}{\partial \mathbf{s}}(\mathbf{r}_0, \mathbf{s}^{(k)}) \delta \mathbf{s}^{(k)}, \\ &= \left(I - \frac{\partial \mathcal{C}_m}{\partial \mathbf{s}}(\mathbf{r}_0, \mathbf{s}^{(k)}) \right) \delta \mathbf{s}^{(k)}, \\ &= -g_m(\mathbf{r}_0, \mathbf{s}^{(k)}), \end{aligned}$$

with $A = \frac{\partial g_m}{\partial \mathbf{s}}$ the linearization (Jacobian matrix) of g_m and $\frac{\partial \mathcal{C}_m}{\partial \mathbf{s}}$ the linearization of \mathcal{C}_m . I represents the identity matrix. The linearization can be estimated with the help of the approximation

$$A\mathbf{e}_i \approx \frac{g_m(\mathbf{r}_0, \mathbf{s} + \varepsilon \mathbf{e}_i) - g_m(\mathbf{r}_0, \mathbf{s})}{\varepsilon}, \quad (3.10)$$

with \mathbf{e}_i the unit vector, $i = 1, \dots, 2n$ and ε small.

3.3. Constrained Runs algorithm applied to general discrete Boltzmann equations. The previous section outlined the application of the Constrained Runs algorithm to a lattice Boltzmann model with three velocities and where only the density, the lowest order velocity moment, is given.

One question is how the method should be applied to other discretizations of the Boltzmann equation, for example the finite volume discretization discussed in section 2.1. These discrete models have many more discrete velocities than the LBM. Consider again a one-dimensional spatial domain. Instead of three, we have N_v velocity directions with velocities represented as $\{v_0, \dots, v_{N_v-1}\}$. Furthermore, the models

can have, besides the density, also momentum, and temperature given as macroscopic variables.

In principle (3.8) is easily generalized to a problem with N_v velocities. The matrix M — the matrix that transforms the distribution functions into velocity moments — is now a transposed Vandermonde matrix

$$M = \begin{pmatrix} 1 & 1 & \dots & 1 & 1 \\ v_0 & v_1 & \dots & v_{q-2} & v_{q-1} \\ v_0^2 & v_1^2 & \dots & v_{q-2}^2 & v_{q-1}^2 \\ \vdots & \vdots & & \vdots & \vdots \\ v_0^{q-1} & v_1^{q-1} & \dots & v_{q-2}^{q-1} & v_{q-1}^{q-1} \end{pmatrix},$$

with $q = N_v$. Define M^0 as

$$M^0 = \begin{pmatrix} 1 & 1 & \dots & 1 & 1 \\ v_0 & v_1 & \dots & v_{q-2} & v_{q-1} \\ \vdots & \vdots & & \vdots & \vdots \\ v_0^{k-1} & v_1^{k-1} & \dots & v_{q-2}^{k-1} & v_{q-1}^{k-1} \\ 0 & 0 & \dots & 0 & 0 \\ \vdots & \vdots & & \vdots & \vdots \\ 0 & 0 & \dots & 0 & 0 \end{pmatrix},$$

with k the number of conserved macroscopic variables, $1 \leq k < N_v$. M^0 represents the part of matrix M that produces the lower order velocity moments which should be conserved in the CR algorithm. The part corresponding to the higher order velocity moments is replaced with zeros. When $k = 3$ we conserve density, momentum, and temperature. These macroscopic variables are linked to the three lowest order velocity moments of the distribution functions.

Since M is a transposed Vandermonde matrix and the inverse of this matrix is required to write down the projection operator in the first term of equation (3.8), we should deal with the inverse of such a matrix.

A lot of literature elaborates on this problem in the context of polynomial interpolation. However, in realistic applications more than hundred velocity directions need to be taken into account. Even with known techniques, like using the Lagrange polynomials for inverting the Vandermonde matrix [20] or by defining the moments in Chebyshev polynomials [12], it is still impossible to compute the inverse with lots of velocity directions. Similarly, the method discussed by Golub and Van Loan in [8] to solve a Vandermonde system by comparing it to polynomial interpolation and considering the Newton representation of the interpolating polynomial has analogous issues.

These issues are further outlined below. When M^{-1} is not computed correctly, the conservation of the given macroscopic variables cannot be guaranteed. This is demonstrated in Example 1 that shows that P is not a projection operator when M^{-1} is computed incorrectly. We deal with these issues in the remainder of this section.

EXAMPLE 1 (Eigenvalues of $P := I - M^{-1}M^0$). *This example shows one of the major issues of inverting matrix M to obtain projection operator P in the CR algorithm. Since P is a projection operator the eigenvalues should be either zero or one. Figure 3.1 contains the computed eigenvalues of this operator with $N_v = 56$,*

$v_{min} = -9.9875 \cdot 10^3$ m/s, $v_{max} = 9.9875 \cdot 10^3$ m/s, and $\Delta v = (v_{max} - v_{min})/N_v$. This figure shows that we lose the property of the eigenvalues being either zero or one.

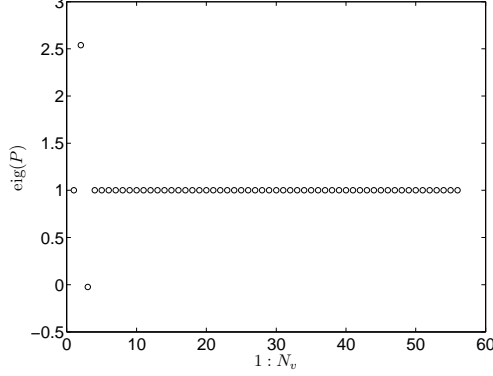


FIG. 3.1. Computed eigenvalues of operator $P = I - M^{-1}M^0$ with $N_v = 56$, $v_{min} = -9.9875 \cdot 10^3$ m/s, $v_{max} = 9.9875 \cdot 10^3$ m/s, and $\Delta v = (v_{max} - v_{min})/N_v$. P should be a projection operator thus we expect the eigenvalues to be either zero or one. This figure shows that we lose this property when using the inverse of matrix M in the numerical experiment.

Example 1 illustrates the difficulties that originate from inverting matrix M . It is clear that the loss of accuracy leads to eigenvalues that deviate from zero or one. This has important consequences for the Constrained Runs algorithm since the conservation of the lower order velocity moments is required. And this is not longer the case with incorrect projection operators.

Example 2 incorporates the Chebyshev polynomials to compute M^{-1} . Similarly, we lose the property of eigenvalues being either zero or one.

EXAMPLE 2 (Eigenvalues of $P := I - M^{-1}M^0$ by defining the moments in Chebyshev polynomials). This example checks the property that P should be a projection operator when P is based on defining the velocity moments in Chebyshev polynomials. Figure 3.2 contains the computed eigenvalues of this operator with $N_v = 56$, $v_{min} = -9.9875 \cdot 10^3$ m/s, $v_{max} = 9.9875 \cdot 10^3$ m/s, and $\Delta v = (v_{max} - v_{min})/N_v$. This figure shows that we lose the property of the eigenvalues being either zero or one.

However, the use of M^{-1} can be circumvented. The projection on the space of higher order moments can be written as a subtraction of the components in the direction of the lower order moments. This then only requires orthogonal vectors that span the space of lower order moments.

Let us look at the QR factorization of $M^{0T}(:, 1:k)$ where k is the number of conserved macroscopic variables:

$$M^{0T}(:, 1:k) = QR,$$

where Q contains k orthogonal columns and R is a k by k upper triangular matrix. When density, momentum, and energy are conserved in a one-dimensional problem R is a 3×3 matrix and Q contains three columns. Let us define $\hat{M}^0 := [Q^T; 0]$. We now have that $M^0(1:k, :) = R^T \hat{M}^0(1:k, :)$. The space spanned by the columns of \hat{M}^0 now spans the same space as the original low order moments.

The CR iteration $\mathbf{f}^{(k+1)} = \hat{P} \mathbf{f}^{(k)\text{pre}} + \hat{M}^0 \mathbf{f}^0$, where \hat{P} projects on the space of the higher order moments, can now be written as

$$\mathbf{f}^{(k+1)} = (1 - \hat{M}^{0T} \hat{M}^0) \mathbf{f}^{(k)\text{pre}} + \hat{M}^0 \mathbf{f}^0, \quad (3.11)$$

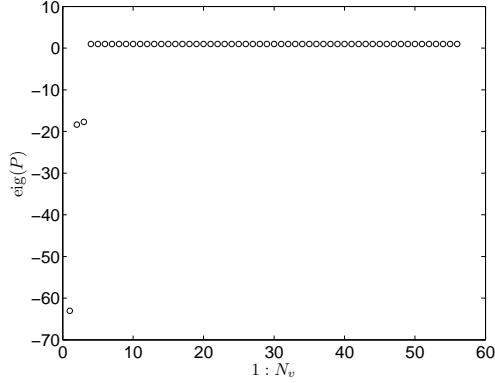


FIG. 3.2. Computed eigenvalues of operator $P = I - M^{-1}M^0$ with $N_v = 56$, $v_{min} = -9.9875 \cdot 10^3$ m/s, $v_{max} = 9.9875 \cdot 10^3$ m/s, and $\Delta v = (v_{max} - v_{min})/N_v$. P should be a projection operator thus we expect the eigenvalues to be either zero or one. This figure shows that we lose this property when using the inverse of matrix M in the numerical experiment when M is based on defining the velocity moments in Chebyshev polynomials.

which avoids the inverse of the moment matrix. (3.11) can be written because $\hat{M}^T \hat{M}^0 = \hat{M}^{0T}(:, 1:k) \hat{M}^0(1:k, :)$, where \hat{M} is the matrix that would have been obtained by a QR factorization of the full moment matrix M .

We will demonstrate that an iteration using \hat{M} will preserve the same moments as the original procedure based on M . However, the procedure based on \hat{M} is more stable, which can be observed from the eigenvalues of the projection operator. Example 3 shows these eigenvalues for a similar numerical experiment as in Example 1 and Example 2.

EXAMPLE 3 (Eigenvalues of $\hat{P} := I - \hat{M}^T \hat{M}^0$). The eigenvalues of \hat{P} should be either zero or one since \hat{P} is a projection operator. Figure 3.3 shows the computed eigenvalues of this operator with $N_v = 56$, $v_{min} = -9.9875 \cdot 10^3$ m/s, $v_{max} = 9.9875 \cdot 10^3$ m/s, and $\Delta v = (v_{max} - v_{min})/N_v$. The property of the eigenvalues being either zero or one is fulfilled for this numerical experiment.

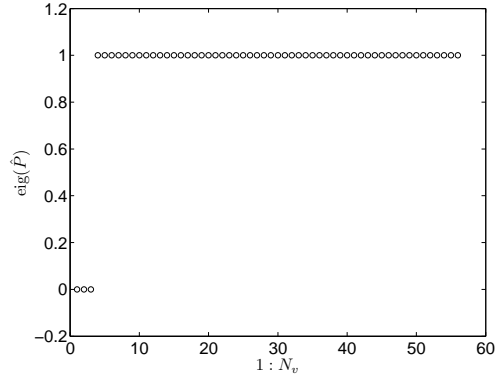


FIG. 3.3. Computed eigenvalues of operator $\hat{P} = I - \hat{M}^T \hat{M}^0$ with $N_v = 56$, $v_{min} = -9.9875 \cdot 10^3$ m/s, $v_{max} = 9.9875 \cdot 10^3$ m/s, and $\Delta v = (v_{max} - v_{min})/N_v$. \hat{P} should be a projection operator thus we expect the eigenvalues to be either zero or one. This figure shows that operator \hat{P} fulfills this property for the numerical experiment.

Example 3 shows that this alternative setting fulfills the property of eigenvalues being zero or one for projection operator \hat{P} . We check the effect of this redefinition — using \hat{P} instead of P — on the CR algorithm.

Now, we check whether this algorithm conserves the same lower order velocity moments, the k conserved macroscopic variables

$$\begin{aligned} M^0(1:k, :)\mathbf{f}^{(k)} &= M^0(1:k, :) \left(\hat{P}\mathbf{f}^{(k)\text{pre}} + (I - \hat{P})\mathbf{f}^0 \right), \\ &= M^0(1:k, :)\hat{P}\mathbf{f}^{(k)\text{pre}} + M^0(1:k, :)\mathbf{f}^0 - M^0(1:k, :)\hat{P}\mathbf{f}^0, \\ &= R^T \hat{M}^0(1:k, :)\hat{P}\mathbf{f}^{(k)\text{pre}} + M^0(1:k, :)\mathbf{f}^0 - R^T \hat{M}^0(1:k, :)\hat{P}\mathbf{f}^0. \end{aligned}$$

The first and last term of the right-hand side vanish because of the definition of the projection space \hat{W} of operator \hat{P} . It follows that

$$M^0(1:k, :)\mathbf{f}^{(k)} = M^0(1:k, :)\mathbf{f}^0.$$

This confirms the correspondence between the lower order moments in the CR algorithm and those of \mathbf{f}^0 , the initial distribution function.

4. Numerical results. We illustrate the proposed method with the help of a model problem coming from laser ablation. Here a Boltzmann model is studied with a left boundary condition that models the evaporation of material from a heated surface, while the right boundary models the ambient gas. We refer to [9] for a detailed discussion of the physics and the Boltzmann model. This section contains numerical results which test the generalized CR algorithm in a setting of restriction and lifting.

EXAMPLE 4 (One-dimensional Helium problem). *As a model problem, we consider the one-dimensional laser ablation problem with Helium as a background gas. The ambient gas parameters p_a, T_a, n_a, ρ_a , and u_a represent the pressure, temperature, number density, mass density, and average flow velocity while p_s, T_s, n_s, ρ_s , and u_s are the surface parameters. These parameters, presented below in (4.1), are used for initialization and to obtain boundary conditions. These are similar to the parameters presented in [9]. The boundary conditions at the surface are based on the equilibrium distribution of the surface parameters while the outer boundary is placed far enough from the interface such that the vapor is in equilibrium there.*

$$\begin{aligned} p_a &= 0.10132500 \cdot 10^6 \text{ Pa}, \quad T_a = 0.30000785 \cdot 10^3 \text{ K}, \quad n_a = \frac{p_a}{k_B T_a}, \\ \rho_a &= m n_a, \quad u_a = 0, \quad p_s = \frac{p_a}{0.3}, \quad T_s = \frac{T_a}{0.2}, \quad n_s = \frac{p_s}{k_B T_s}, \\ \rho_s &= m n_s, \quad u_s = 0. \end{aligned} \tag{4.1}$$

We focus on the finite volume discretization, outlined in section 2.1, with discretization parameters listed below in (4.2).

$$\begin{aligned}
N &= 1600, \quad N_v = 56, \quad u_0 = \sqrt{\frac{2k_B T_s}{m}}, \quad v_{min} = -4u_0, \quad v_{max} = 4u_0, \\
\Delta v &= \frac{v_{max} - v_{min}}{N_v}, \quad \mathbf{v} = \left[v_{min} + \frac{\Delta v}{2} : \Delta v : v_{max} - \frac{\Delta v}{2} \right], \quad \lambda = \frac{1}{\sqrt{2}\pi d^2 n_s}, \\
L &= 30000\lambda, \quad h = \frac{L}{N}, \quad \mathbf{x} = \left[\frac{h}{2} : h : \frac{h}{2} + (N-1)h \right], \\
\mu_{ref} &= 0.19 \cdot 10^{-4} \text{ Pa} \cdot \text{s}, \quad T_{ref} = 273.15 \text{ K}, \quad \omega(\mathbf{x}, t) = \frac{\rho(\mathbf{x}, t) k_B / m T(\mathbf{x}, t)}{\mu_{ref} (T(\mathbf{x}, t) / T_{ref})^{0.66}}, \\
\Delta t &= 0.9 \frac{1}{\max(\mathbf{v})/h + \max(\omega(\mathbf{x}, 0))}, \tag{4.2}
\end{aligned}$$

with d the gas-kinetic molecular diameter and λ the mean free path. The time step Δt is defined in such a way for stability reasons [17].

Since the length of the domain determines the discretization parameters, we can also consider

$$L = 30\lambda, \tag{4.3}$$

which is a valid choice for the length since the thickness of the nonequilibrium layer is about 10-20 mean free path lengths [9]. The remaining discretization parameters are the same as those presented in (4.2).

These different domain lengths determine the possibility of using the CR algorithm as a lifting operator. This is one of the issues discussed in section 4.1, which is related to the convergence rate of CR.

4.1. Comparison of P and \hat{P} in the CR algorithm. The following illustrates the issues of using the inverse of matrix M in the projection operator of the Constrained Runs algorithm. Figure 4.1 shows both the spectra of the Jacobian matrices of the CR map with operators P , which uses the inverse of M , and \hat{P} , which avoids this inverse, respectively in the left and right figure. The spectra correspond to a Constrained Runs algorithm with $m = 0$. The eigenvalues should remain within the unit circle for the algorithm to be stable. Since we are focusing on a generalization of Constrained Runs, we are not only taking the density as a given macroscopic variable but also average flow velocity and temperature. This example includes 56 discrete velocities while preserving the three lowest order velocity moments for the Helium problem presented in Example 4. The number of grid points is $N = 200$ as opposed to the general parameters presented in (4.2). This reduction in the number of variables is necessary to make the computation of the Jacobian matrix of the CR map possible.

These figures show a clear stability with projection operator \hat{P} while an instability occurs when using the CR algorithm with P due to the difficulties of computing the inverse of M .

Another issue that is illustrated by the spectrum of the Jacobian matrix of the CR algorithm is the convergence rate of Constrained Runs. Figure 4.2 shows the spectrum of the Helium model problem presented in Example 4 with parameters listed in (4.3), where the ratio of the grid distance Δx to the mean free path is reduced. Again, the CR algorithm with operator P shows a clear instability while \hat{P} stabilizes the method.

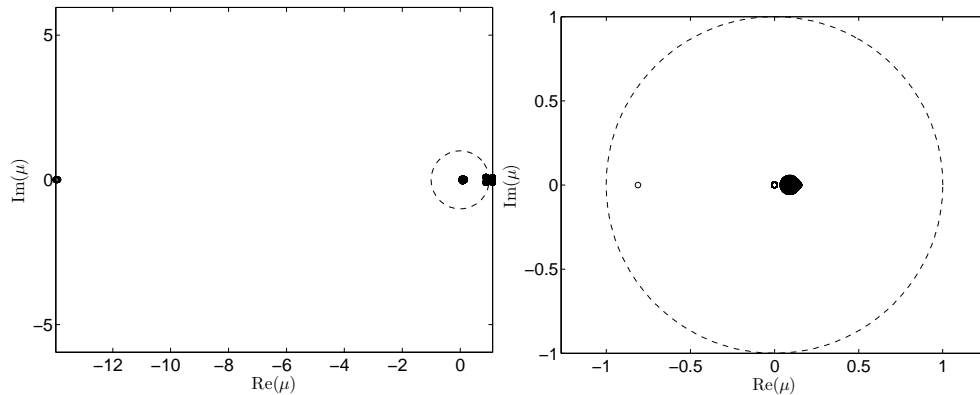


FIG. 4.1. The spectrum of the Jacobian matrix of the Constrained Runs map with $m = 0$. The left figure uses operator P while the right figure is based on projection operator \bar{P} . The parameters are listed in (4.2) of Example 4 with a smaller number of grid points, namely $N = 200$, to make the computation of the Jacobian matrix possible. The unit circle, which should contain the eigenvalues to obtain a stable method, is shown in dashed lines. A clear instability occurs in the left figure when the original projection operator $P = 1 - M^{-1}M^0$ is used in the CR algorithm.

However, the convergence is slower with these parameters since the spectral radius, or equivalently the asymptotic convergence factor, is larger in Figure 4.2 compared to Figure 4.1.

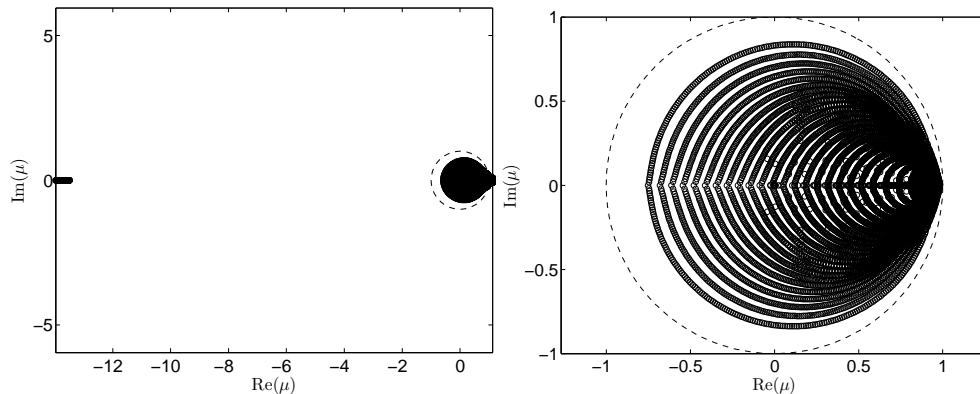


FIG. 4.2. Similar as Figure 4.1 but now with parameters listed in (4.3), where there ratio of Δx to the mean free path is much smaller.

4.2. Test Constrained Runs algorithm in Example 4. This section tests the Constrained Runs algorithm on the model problem presented in Example 4. We perform 10000 Boltzmann time steps on the initial state based on the ambient parameters presented in Example 4 and parameters listed in (4.2). The distribution functions are rescaled with the mass m for numerical reasons due too small numbers to perform the numerics on. This results in a reference distribution function f_c that is plotted in Figure 4.3. As can be seen, a traveling wave emerges in the domain. The corresponding equilibrium distribution is f^{eq} .

We test the CR algorithm as a lifting operator that maps density, average flow velocity, and temperature to distribution functions. The CR algorithm is combined

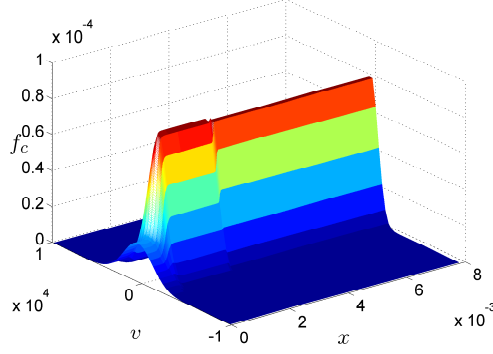


FIG. 4.3. Plot of the reference distribution function \mathbf{f}_c obtained after 10000 time steps on the initial state with parameters presented in Example 4. A traveling wave emerges in the domain. The left boundary condition models the evaporating material in laser ablation. The right boundary is determined by the parameters of the ambient gas. The vertical axis is rescaled with the mass for numerical reasons as described in the text.

with Newton's method to ensure stability. It uses a GMRES algorithm to estimate the Jacobian matrix in Newton's method. The parameters of the GMRES algorithm are default parameters in Matlab. The convergence of GMRES might be improved if a preconditioner is used similar to [13].

The lifting operator can be evaluated by restricting the reference distribution function \mathbf{f}_c to its macroscopic variables and lift them back to a distribution function \mathbf{f} by using the lifting operator. The resulting \mathbf{f} is compared with \mathbf{f}_c with the help of the two-norm $\|\mathbf{f} - \mathbf{f}_c\|$, which is shown in Table 4.1. These results can be compared to $\|\mathbf{f}^{eq} - \mathbf{f}_c\|$ which is equal to 6.4940e-007. They are based on Newton's method with a tolerance value of 1.0e-010. It might improve with a stricter tolerance.

TABLE 4.1

The error $\|\mathbf{f} - \mathbf{f}_c\|$ to test the CR algorithm as a lifting operator (combined with Newton's method) for various orders of accuracy. The reference distribution function \mathbf{f}_c is obtained for the model problem in Example 4 by performing 10000 Boltzmann time steps on the initial state.

Order CR	$\ \mathbf{f} - \mathbf{f}_c\ $
0	1.0428e-006
1	1.6413e-008
2	6.1629e-010
3	4.1965e-010

Figure 4.4 presents a log plot of the relative errors $\left| \frac{\mathbf{f}^{eq} - \mathbf{f}_c}{\mathbf{f}_c} \right|$ (top left) and $\left| \frac{\mathbf{f} - \mathbf{f}_c}{\mathbf{f}_c} \right|$. These results are plotted in function of spatial grid points \mathbf{x} and velocities \mathbf{v} . \mathbf{f} corresponds to the distribution functions based on lifting with the Constrained Runs algorithm of order $m = 0$ (top right), $m = 1$ (middle left), $m = 2$ (middle right), $m = 3$ (bottom left), and $m = 4$ (bottom right). We show a narrow range of velocity directions since the outer velocities bring the distribution functions to zero. Where the figures show no results (white area in figures), $|\mathbf{f} - \mathbf{f}_c|$ is exactly equal to zero, which makes it impossible to create the log plot.

Furthermore, we plot $\sum_i |\mathbf{f}_i^{eq} - (\mathbf{f}_c)_i|$ and $\sum_i |\mathbf{f}_i - (\mathbf{f}_c)_i|$ in Figure 4.5 to get an idea on the construction of the hybrid domain.

This suggests the use of a Boltzmann model near the traveling wave while a PDE

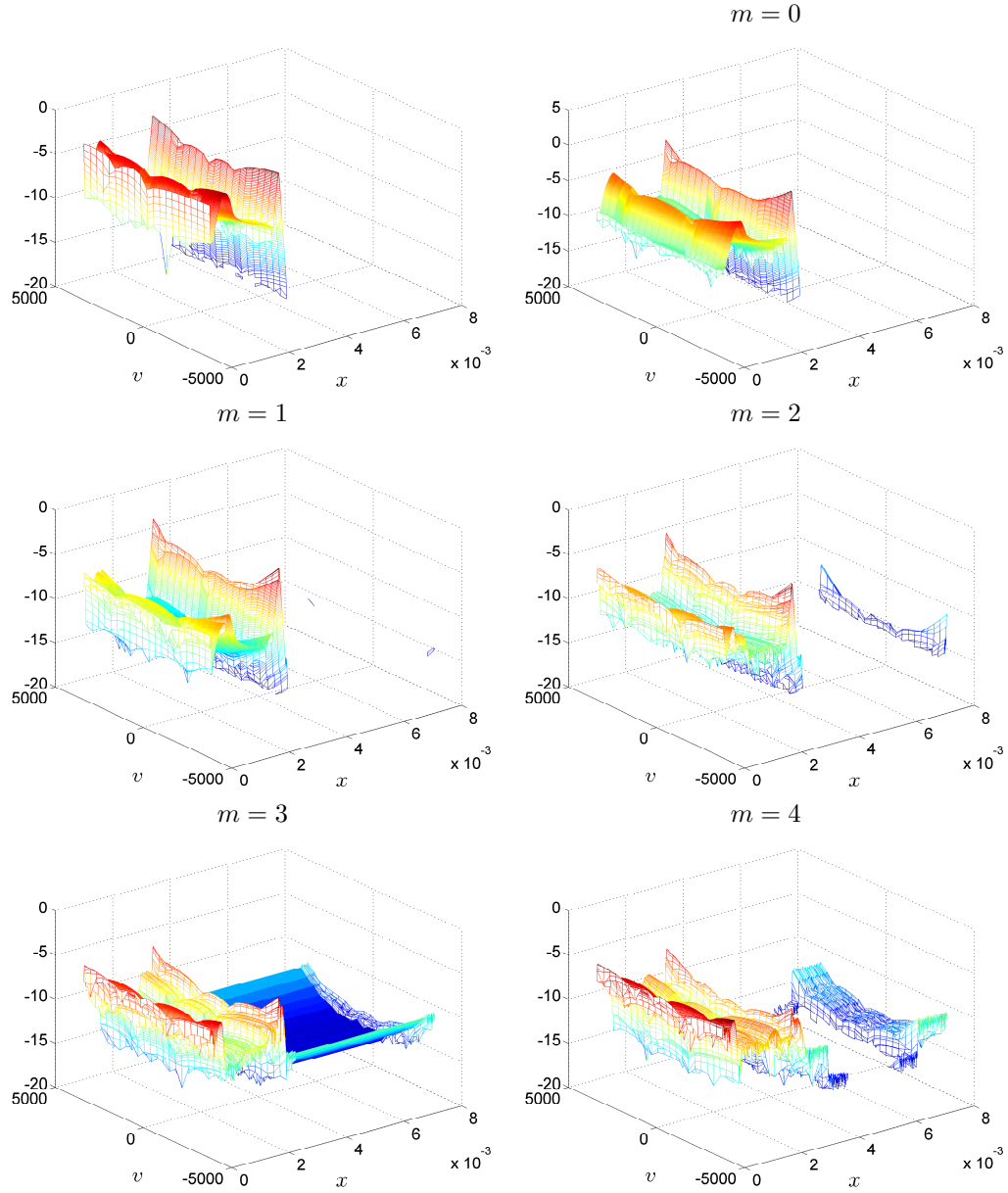


FIG. 4.4. Log plot of the relative error $\left| \frac{f^{eq} - f_c}{f_c} \right|$ (top left) and similarly of $\left| \frac{f - f_c}{f_c} \right|$ where f_c represents the reference distribution function after 10000 time steps on the initial state with parameters presented in Example 4. f^{eq} is the corresponding equilibrium distribution after 10000 steps and f the distribution functions based on lifting with the Constrained Runs algorithm of order $m = 0$ (top right), $m = 1$ (middle left), $m = 2$ (middle right), $m = 3$ (bottom left), and $m = 4$ (bottom right). Where the figures show no results (white area in figures), $|f - f_c|$ is exactly equal to zero, which makes it impossible to create the log plot.

domain can be used outside this part of the domain. Extra care is also needed at the boundaries where the surface parameters determine the state.

EXAMPLE 5 (Helium problem including radial velocities). *This example considers the laser ablation problem from [9] with Helium as a background gas in a three-dimensional domain described through radial velocities, which represent the axial symmetry. p_a, T_a, n_a, ρ_a , and u_a again correspond to the ambient parameters pressure, temperature, number density, mass density, and average flow velocity while p_s, T_s, n_s, ρ_s , and u_s are the surface parameters which are given below. These are similar to the parameters presented in [9].*

$$\begin{aligned} p_a &= 0.10132500 \cdot 10^6 \text{ Pa}, \quad T_a = 0.30000785 \cdot 10^3 \text{ K}, \quad n_a = \frac{p_a}{k_B T_a}, \\ \rho_a &= m n_a, \quad u_a = 0, \quad p_s = \frac{p_a}{0.3}, \quad T_s = \frac{T_a}{0.2}, \quad n_s = \frac{p_s}{k_B T_s}, \\ \rho_s &= m n_s, \quad u_s = 0. \end{aligned}$$

The discrete distribution function is defined on a two-dimensional grid with velocities $(v_z)_i = (v_z)_0 + i \Delta v_z$, $i \in \{0, \dots, N_z - 1\}$ and $(v_r)_{i'} = (v_r)_0 + i' \Delta v_r$, $i' \in \{0, \dots, N_r - 1\}$, specified in the cylindrical domain of the velocity space with $(v_z)_{\min} < v_z < (v_z)_{\max}$ and $0 < v_r < (v_r)_{\max}$. $v_r = [(v_x)^2 + (v_y)^2]^{1/2}$ is the radial velocity, which takes into account the axial symmetry. The axial and radial velocity increments are $\Delta v_z = ((v_z)_{\max} - (v_z)_{\min})/N_z$ and $\Delta v_r = (v_r)_{\max}/N_r$, respectively, $(v_z)_0 = (v_z)_{\min} + \Delta v_z/2$ and $(v_r)_0 = \Delta v_r/2$. The discretization parameters now correspond to

$$\begin{aligned} N &= 1600, \quad N_z = 56, \quad N_r = 24, \quad u_0 = \sqrt{\frac{2k_B T_s}{m}}, \\ (v_z)_{\min} &= -4u_0, \quad (v_z)_{\max} = 4u_0, \quad \Delta v_z = \frac{(v_z)_{\max} - (v_z)_{\min}}{N_z}, \\ \mathbf{v}_z &= \left[(v_z)_{\min} + \frac{\Delta v_z}{2} : \Delta v_z : (v_z)_{\max} - \frac{\Delta v_z}{2} \right], \quad (v_r)_{\min} = 0, \\ (v_r)_{\max} &= 3u_0, \quad \Delta v_r = \frac{(v_r)_{\max}}{N_r}, \quad \mathbf{v}_r = \left[\frac{\Delta v_r}{2} : \Delta v_r : (v_r)_{\max} - \frac{\Delta v_r}{2} \right], \\ \lambda &= \frac{1}{\sqrt{2}\pi d^2 n_s}, \quad L = 30000\lambda, \quad h = \frac{L}{N}, \quad \mathbf{z} = \left[\frac{h}{2} : h : \frac{h}{2} + (N-1)h \right], \\ \mu_{\text{ref}} &= 0.19 \cdot 10^{-4} \text{ Pa} \cdot \text{s}, \quad T_{\text{ref}} = 273.15 \text{ K}, \quad \omega(\mathbf{z}, t) = \frac{\rho(\mathbf{z}, t) k_B / m T(\mathbf{z}, t)}{\mu_{\text{ref}} (T(\mathbf{z}, t) / T_{\text{ref}})^{0.66}}, \\ \Delta t &= 0.9 \frac{1}{\max(\mathbf{v}_z)/h + \max(\omega(\mathbf{z}, 0))}. \end{aligned} \tag{4.4}$$

Including radial velocities requires a redefinition of the velocity moment matrix M . In general, tensors are necessary to describe higher order velocity moments [18]. The lower order moments, density, average flow velocity, and temperature are given in (2.2).

We start by checking the eigenvalues of \hat{P} with this extended moment matrix. The eigenvalues should still be either zero or one since \hat{P} is a projection operator. Figure 4.6 shows the computed eigenvalues of this operator for Example 5 which shows only eigenvalues equal to zero or one.

4.3. Test Constrained Runs algorithm in Example 5. This section tests the Constrained Runs algorithm on the model problem presented in Example 5. It is

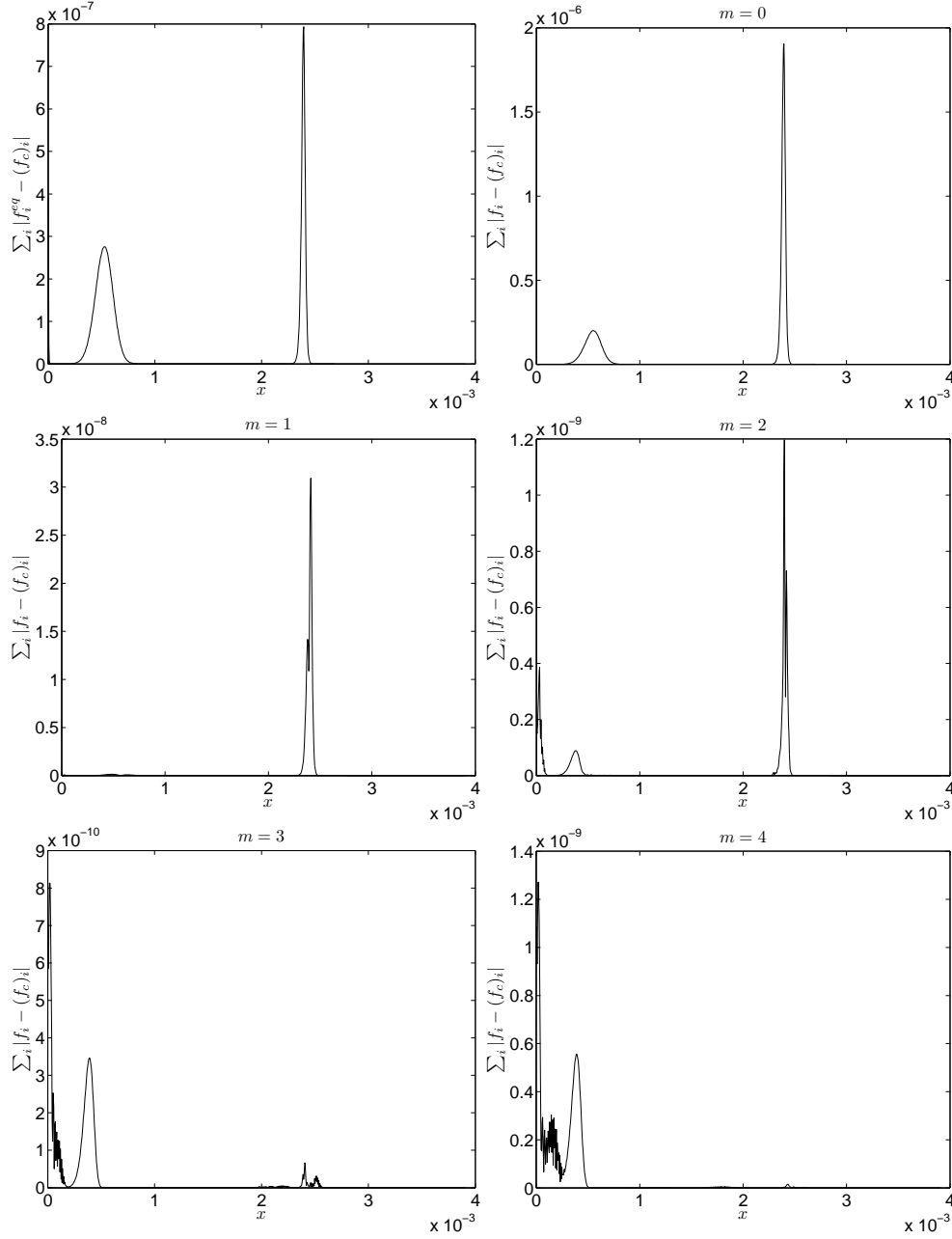


FIG. 4.5. Plot of the absolute differences $\sum_i |f_i^{eq} - (f_c)_i|$ (top left) and $\sum_i |f_i - (f_c)_i|$ where f_c represents the reference distribution function after 10000 time steps on the initial state with parameters presented in Example 4. f^{eq} is the corresponding equilibrium distribution and f the distribution functions based on lifting with the Constrained Runs algorithm of order $m = 0$ (top right), $m = 1$ (middle left), $m = 2$ (middle right), $m = 3$ (bottom left), and $m = 4$ (bottom right). Note the different scales in the figures. These figures are shown to get an idea on the construction of the hybrid domain.

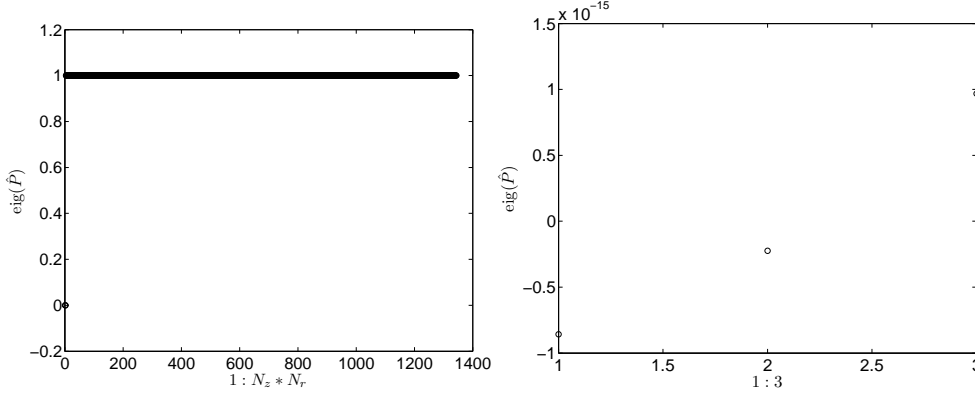


FIG. 4.6. Computed eigenvalues of operator $\hat{P} = I - \hat{M}^T \hat{M}^0$ (left) with $N_z = 56$ and $N_r = 24$ as presented in Example 5. \hat{P} should be a projection operator thus we expect the eigenvalues to be either zero or one. We see, by investigating the region around zero, that operator \hat{P} fulfills this property (right).

based on parameters suggested by Gusarov et al. [9] for the laser ablation problem. The boundary conditions of the Boltzmann discretization are equilibrium distributions of the surface parameters at the surface and equilibrium distributions of the ambient parameters at the outer boundary. We perform 10000 Boltzmann time steps on the initial state based on the ambient parameters presented in Example 5. The distribution functions are rescaled with the mass m and weights $2\pi\Delta v_z\Delta v_r$, corresponding to the radial velocity directions. The traveling wave that emerges in the domain moves from the surface, on the left, towards the ambient boundary, at the right. The resulting reference distribution function is denoted as \mathbf{f}_c . The corresponding equilibrium distribution is denoted as \mathbf{f}^{eq} .

We test the performance of the CR algorithm as a lifting operator that maps density, average flow velocity, and temperature to distribution functions. The CR algorithm is combined with Newton's method to ensure stability. It uses a GMRES algorithm to invert the Jacobian matrix in Newton's method and the matrix-vector product of the Jacobian matrix is estimated using finite differences.

Figure 4.7 presents a log plot of the relative errors $\left| \frac{\mathbf{f}^{eq} - \mathbf{f}_c}{\mathbf{f}_c} \right|$ (top left) and $\left| \frac{\mathbf{f} - \mathbf{f}_c}{\mathbf{f}_c} \right|$. These results are plotted in function of spatial grid points \mathbf{z} and velocities in the z -direction \mathbf{v}_z . \mathbf{f} corresponds to the distribution function based on lifting with the Constrained Runs algorithm of order $m = 0$ (top right), $m = 1$ (bottom left), and $m = 2$ (bottom right). It shows a narrow range of velocity directions \mathbf{v}_z since the outer velocities bring the distribution functions to zero. Furthermore, the results include radial velocities \mathbf{v}_r . The errors are based on sums of distribution functions over the different radial velocity directions.

There are two remarks that illustrate the drawbacks of the Constrained Runs algorithm.

REMARK 1. A serious drawback is the dependence of the convergence rate of the Constrained Runs algorithm on the parameters of the Boltzmann model. This is illustrated in Figures 4.1 and 4.2. This makes it computationally not feasible to use the CR algorithm as a lifting operator for certain choices of the parameters of the Boltzmann model, especially when the grid resolution is smaller than the mean free path. This is illustrated in Figure 4.8, where the number of outer GMRES iterations

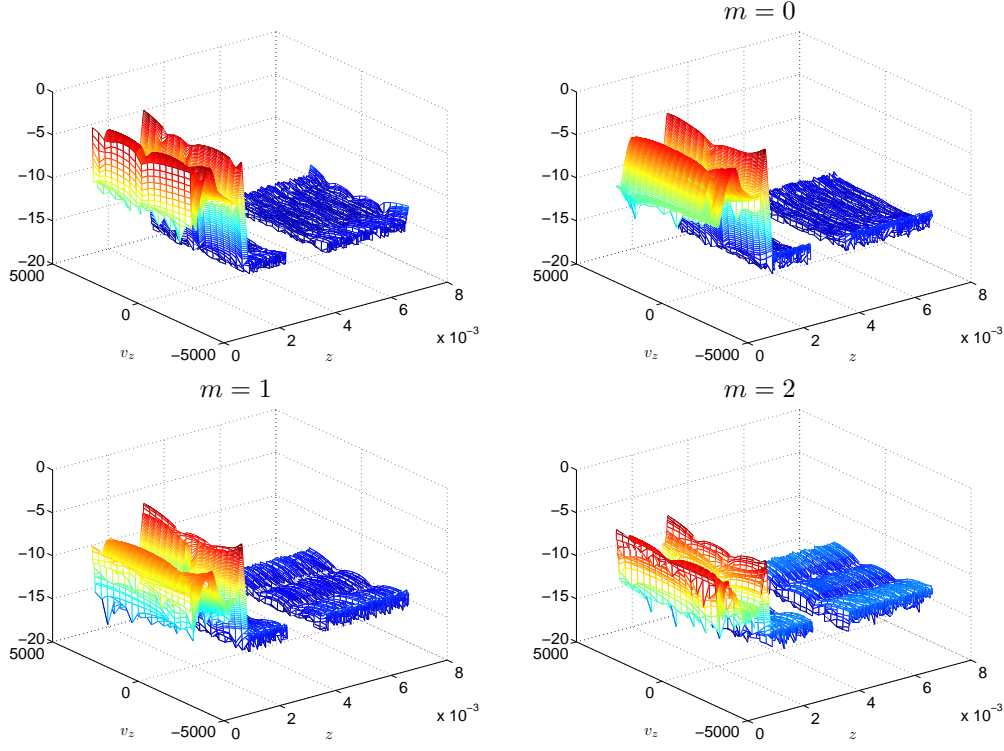


FIG. 4.7. Log plot of the relative error $\left| \frac{f^{eq} - f_c}{f_c} \right|$ (top left) and similarly of $\left| \frac{f - f_c}{f_c} \right|$ where f_c represents the reference distribution function after 10000 time steps on the initial state with parameters presented in Example 5. f^{eq} is the corresponding equilibrium distribution and f the distribution functions based on lifting with the Constrained Runs algorithm of order $m = 0$ (top right), $m = 1$ (bottom left), and $m = 2$ (bottom right). Furthermore, the results include radial velocities v_r . The errors are based on sums of distribution functions over the different radial velocity directions.

is shown in function of N , the number of spatial grid points for $m = 0$ (circle), $m = 1$ (asterisk), $m = 2$ (plus sign), $m = 3$ (point), $m = 4$ (cross), and $m = 5$ (triangle). It is clear that the convergence rate of CR is determined by the parameters of the Boltzmann model, especially the ratio of Δx to the mean free path λ , is important.

To obtain a good convergence rate of Constrained Runs in the previous examples, we chose the length of the domain $L = 30000\lambda$ in (4.2) and (4.4). We would rather like to have $L = 30\lambda$ such that the nonequilibrium layer is well described. It typically has a thickness of 10 to 20 mean free path lengths [9]. This means that the current grid step equal to $H = 30000\lambda/N$ has to be reduced to $h = 30\lambda/N$. This can be interpreted as refinements from Boltzmann_H to Boltzmann_h.

However, to refine Boltzmann models additional operators are necessary that transfer information between different scales. There is some literature on the coupling of lattice Boltzmann models with different grid resolutions. Guzik et al. present a space-time interpolation method to couple different grid resolutions for lattice Boltzmann models [10, 11]. Here the first nonequilibrium term is matched between the two Boltzmann models.

There is no literature for general discrete Boltzmann models with multiple velocities, to the best of our knowledge.

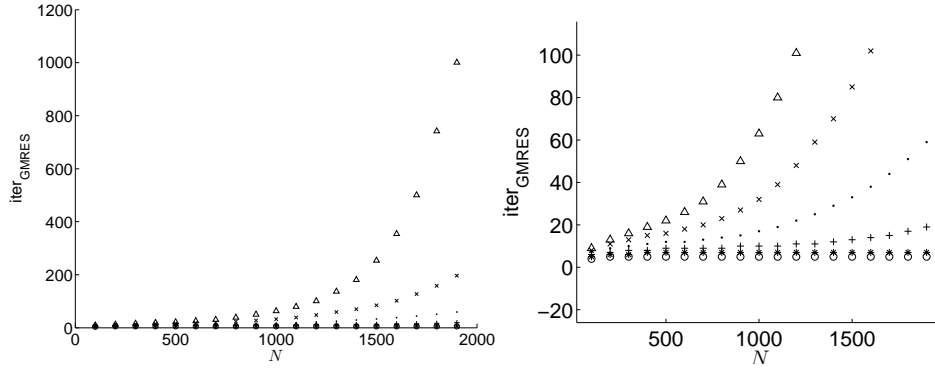


FIG. 4.8. Plot of the number of outer GMRES iterations in function of N , the number of spatial grid points for $m = 0$ (circle), $m = 1$ (asterisk), $m = 2$ (plus sign), $m = 3$ (point), $m = 4$ (cross), and $m = 5$ (triangle). with parameters presented in Example 4. The plot on the right represents a zoom of the left figure. This shows that the convergence rate of CR depends on the parameters of the Boltzmann model.

If it is possible to transfer between the Boltzmann subdomains with different grid sizes, denoted Boltzmann_H and Boltzmann_h , then the following scenario would be possible.

First, there is a lifting operator that transfers information between Boltzmann_H and PDE_H where H is large. This has the advantage that this is better for the convergence rate of the Constrained Runs algorithm since the grid sizes determine the spectral radius as highlighted in section 4.1. Then the Boltzmann model is systematically refined to reach the correct resolution to resolve the non-equilibrium layer. An overall analysis is required to maintain the accuracy at each boundary.

REMARK 2. Another drawback of the CR algorithm in general is the computational expense since it is based on performing Boltzmann steps to determine the Jacobian matrix in Newton's method. In a similar way, when a matrix-free method is used such as GMRES the convergence is slow without preconditioning.

REMARK 3. The Knudsen number K_n , which is the ratio of the mean free path and the feature length, is often used to classify flow regimes [18]:

- $K_n < 0.01$: hydrodynamic regime,
- $0.01 < K_n < 0.1$: slip flow regime,
- $0.1 < K_n < 10$: transition regime,
- $K_n > 10$: free molecular flow.

This classification is used as a rule of a thumb to determine which mathematical description is necessary.

In laser ablation, the surface gets hot and ejects particles. At the surface a nonequilibrium layer emerges that requires a full Boltzmann description. While away from the surface, a PDE model can be used to simulate the flow. Under what conditions can we lift information from the PDE model to information required by the Boltzmann model? Can this be linked to the classification with the Knudsen number?

To know the link between the microscopic Boltzmann model and the macroscopic PDE models, a Chapman–Enskog expansion is used. This assumes that the Knudsen number is a small parameter (to achieve the Navier–Stokes equations). Indeed, in the hydrodynamic regime, the Knudsen number is a small parameter.

This Knudsen number should help us to determine the conditions when to switch

from Boltzmann to PDE model in the hybrid domain. However, this is, so far, not investigated in detail since the Knudsen number depends on the feature length that is hard to estimate from region to region in the domain.

5. Conclusions. Many problems based on the Boltzmann equation require the conversion of moments to the corresponding distribution function. One motivating example is laser ablation where a material plume is ejected from a melting material that is heated by a laser. To describe this process accurately a lifting operator is required that maps hydrodynamic moments, namely density, average flow velocity, and temperature, to distribution functions of the kinetic Boltzmann model at the interface between the melted material and the gas.

This paper extends the applicability of the Constrained Runs (CR) algorithm that lifts these moments to distribution functions to general discretizations of the Boltzmann equation. Previously the CR algorithm was only used to lift lattice Boltzmann models, where it initializes or couples different models together. In this paper, we have focused on lifting with CR in a finite volume discretization of the Boltzmann equation, but we believe that the results of the CR algorithm can be applied to different discretizations.

The main difficulty encountered in this paper is that the straightforward formulation of CR for Boltzmann models requires the inverse of the moment matrix. This is a very ill-conditioned matrix with the properties of a Vandermonde matrix and traditional numerical methods to invert this matrix fail. In this paper we have reformulated the algorithm such that this inversion can be avoided all together.

With this new formulation the method can conserve multiple macroscopic variables and include multiple velocity directions. The paper includes numerical results that test the restriction and lifting. We perform 10000 Boltzmann time steps on the initial state of the laser ablation problem to create a reference distribution function. This reference solution is restricted to its macroscopic variables, density, average flow velocity, and temperature, and lifted back to distribution functions to test the generalized CR algorithm. The error with the original reference distribution can now be reduced by increasing the order of the CR algorithm.

A remaining drawback of the CR algorithm is the computational cost since it is based on the time scale that a Boltzmann simulation needs to reach the slow manifold. Another drawback is the dependence of the convergence rate of CR on the parameters of the Boltzmann domain: length of the domain expressed as mean free path lengths, step sizes, . . .

In [28] and [29] we have applied, for LBMs, the CR on distribution functions represented as the first few terms of the Chapman–Enskog expansion. The iteration then determines the coefficients of the expansion rather than the distribution function itself. This significantly reduces the size of the problem and makes it easy to solve the implicit, higher order problems. In the future, it might be possible to apply this technique for general discretizations of Boltzmann models where multiple moments are conserved since this paper generalized the underlying CR algorithm. However, when a general Maxwell–Boltzmann equilibrium is used and multiple moments are given, the Chapman–Enskog expansion becomes very complicated with the derivatives of the various moments. At this moment it is unclear if this numerical Chapman–Enskog technique is applicable in this context.

Acknowledgments. This work is supported by research project *Hybrid macroscopic and microscopic modelling of laser evaporation and expansion*, G.017008N, funded by ‘Fonds Wetenschappelijk Onderzoek’ together with an ‘ID-beurs’ of the

University of Antwerp. Furthermore, we would like to thank Annemie Bogaerts and David Autrique of the Plasmant group of the University of Antwerp for their help in defining a model problem for the laser ablation problem.

REFERENCES

- [1] K. AOKI, P. DEGOND, L. MIEUSSENS, Numerical simulations of rarefied gases in curved channels: thermal creep, circulating flow and pumping effect, *Commun. Comput. Phys.*, 6 (2009), pp. 919-954.
- [2] G.A. BIRD, *Molecular gas dynamics and the direct simulation of gas flows*, Oxford Sci. Publ., 1994.
- [3] A. BOGAERTS, Z. CHEN, R. GIJBELS, A. VERTES Laser ablation for analytical sampling: what can we learn from modeling?, *Spectrochimica Acta Part B*, 58 (2003), pp. 1867-1893.
- [4] S. CHAPMAN, T.G. COWLING, *The mathematical theory of non-uniform gases*, Cambridge University Press, Cambridge, 1953.
- [5] A.J. CHORIN, J.E. MARSDEN, *A mathematical introduction to fluid mechanics*, Springer-Verlag, 2000.
- [6] W. E, B. ENGQUIST, The heterogeneous multiscale methods, *Comm. Math. Sci.*, 1 (2003), pp. 87-132.
- [7] C.W. GEAR, T.J. KAPER, I.G. KEVREKIDIS, A. ZAGARIS, Projecting to a slow manifold: singularly perturbed systems and legacy codes, *SIAM J. Appl. Dyn. Syst.*, 4 (2005), pp. 711-732.
- [8] G.H. GOLUB, C.F. VAN LOAN, *Matrix computations*, The Johns Hopkins University Press, 1996.
- [9] A.V. GUSAROV, I. SMUROV, Gas-dynamic boundary conditions of evaporation and condensation: numerical analysis of the Knudsen layer, *Physics of Fluids*, 14 (2002), pp. 4242-4255.
- [10] S.M.J. GUZIK, X. GAO, T. WEISGRABER, B. ALDER, P. COLELLA, An adaptive mesh refinement strategy with conservative space-time coupling for the lattice-Boltzmann method, *American Institute of Aeronautics and Astronautics*, 2013.
- [11] S.M. GUZIK, T.H. WEISGRABER, P. COLELLA, B.J. ALDER, Interpolation methods and the accuracy of lattice-Boltzmann mesh refinement, *J. Comput. Phys.*, 259 (2014), pp. 461-487.
- [12] U.W. HOCHSTRASSER, Orthogonal polynomials, In *Handbook of mathematical functions: with formulas, graphs, and mathematical tables*, editors M. Abramowitz, I.A. Stegun, Dover Publications, 1972.
- [13] J. HUANG, C. YANG, X.-C. CAI, Simulation of cavity flows by an implicit domain decomposition algorithm for the discrete-velocity BGK model of the Boltzmann equation, *Lect. Notes Comput. Sci. Eng.*, 2014 (submitted).
- [14] M. JUNK, A. KLAR, L. LUO, Asymptotic analysis of the lattice Boltzmann equation, *J. Comput. Phys.*, 210 (2005), pp. 676-704.
- [15] I.G. KEVREKIDIS, C.W. GEAR, J.M. HYMAN, P.G. KEVREKIDIS, O. RUNBORG, C. THEODOROPOULOS, Equation-free, coarse-grained multiscale computation: enabling microscopic simulators to perform system-level analysis, *Commun. Math. Sci.*, 1 (2003), pp. 715-762.
- [16] P. LAFITTE, G. SAMAËY, Asymptotic-preserving projective integration schemes for kinetic equations in the diffusion limit, *SIAM J. Sci. Comput.*, 34 (2012), pp. 579-602.
- [17] L. MIEUSSENS, Discrete velocity model and implicit scheme for the BGK equation of rarefied gas dynamics, *Math. Models Methods Appl. Sci.*, 10 (2000), pp. 1121-1149.
- [18] H. STRUCHTRUP, *Macroscopic transport equations for rarefied gas flows: approximation methods in kinetic theory*, Springer, 2005.
- [19] S. SUCCI, *The lattice Boltzmann equation for fluid dynamics and beyond*, Oxford University Press, Oxford, 2001.
- [20] L.R. TURNER, Inverse of the Vandermonde matrix with applications, Technical Report, NASA, 1966.
- [21] R.G.M. VAN DER SMAN, M.H. ERNST, Convection-diffusion lattice Boltzmann scheme for irregular lattices, *J. Comput. Phys.*, 160 (2000), pp. 766782.
- [22] P. VAN LEEMPUT, Multiscale and equation-free computing for lattice Boltzmann models, PhD thesis, K.U. Leuven, 2007.
- [23] P. VAN LEEMPUT, C. VANDEKERCKHOVE, W. VANROOSE, D. ROOSE, Accuracy of hybrid lattice Boltzmann/finite difference schemes for reaction-diffusion systems, *Multiscale Model. Simul.*, 6 (2007), pp. 838-857.
- [24] P. VAN LEEMPUT, W. VANROOSE, D. ROOSE, Mesoscale analysis of the equation-free Constrained Runs initialization scheme, *Multiscale Model. Simul.*, 6 (2007), pp. 1234-1255.

- [25] C. VANDEKERCKHOVE, Macroscopic simulation of multiscale systems within the equation-free framework, PhD thesis, K.U. Leuven, 2008.
- [26] C. VANDEKERCKHOVE, I. KEVREKIDIS, D. ROOSE, An efficient Newton–Krylov implementation of the Constrained Runs scheme for initializing on a slow manifold, *J. Sci. Comput.*, 39 (2009), pp. 167-188.
- [27] Y. VANDERHOYDONC, W. VANROOSE, Lifting in hybrid lattice Boltzmann and PDE models, *Comput. Vis. Sci.*, 14 (2011), pp. 67-78.
- [28] Y. VANDERHOYDONC, W. VANROOSE, Numerical extraction of a macroscopic PDE and a lifting operator from a lattice Boltzmann model, *Multiscale Model. Simul.*, 10 (2012), pp. 766-791.
- [29] Y. VANDERHOYDONC, W. VANROOSE, Initialization of lattice Boltzmann models with the help of the numerical Chapman–Enskog expansion, *Procedia Computer Science*, 18 (2013), pp. 1036-1045.
- [30] Y. VANDERHOYDONC, W. VANROOSE, C. VANDEKERCKHOVE, P. VAN LEEMPUT, D. ROOSE, Numerical lifting for lattice Boltzmann models. In *Novel trends in lattice-Boltzmann methods*, volume 3 of *Progress in Computational Physics*, editor M. Ehrhardt, pp. 127-154, Bentham Science Publishers, 2013.
- [31] D.A. WOLF - GLADROW, *Lattice-gas cellular automata and lattice Boltzmann models*, Springer, Berlin, 2000.